

# Persistent Charge Density Wave Memory in a Cuprate Superconductor

X. M. Chen,<sup>1,\*</sup> C. Mazzoli,<sup>2</sup> Y. Cao,<sup>1</sup> V. Thampy,<sup>1,†</sup> A. M. Barbour,<sup>2</sup> W. Hu,<sup>2</sup> M. Lu,<sup>3</sup> T. Assefa,<sup>1</sup> H. Miao,<sup>1</sup> G. Fabbris,<sup>1</sup> G. D. Gu,<sup>1</sup> J. M. Tranquada,<sup>1</sup> M. P. M. Dean,<sup>1,‡</sup> S. B. Wilkins,<sup>2,§</sup> and I. K. Robinson<sup>1,4,¶</sup>

<sup>1</sup>*Condensed Matter Physics and Materials Science Department,  
Brookhaven National Laboratory, Upton, New York 11973, USA*

<sup>2</sup>*National Synchrotron Light Source II, Brookhaven National Laboratory, Upton, New York 11973, USA*

<sup>3</sup>*Center for Functional Nanomaterials, Brookhaven National Laboratory, Upton, New York 11973, USA*

<sup>4</sup>*London Centre for Nanotechnology, University College, Gower St., London, WC1E 6BT, UK*

(Dated: April 5, 2022)

Although charge density wave (CDW) correlations appear to be a ubiquitous feature of the superconducting cuprates, their disparate properties suggest a crucial role for coupling or pinning of the CDW to lattice deformations and disorder. While diffraction intensities can demonstrate the occurrence of CDW domain formation, the lack of scattering phase information has limited our understanding of this process. Here, we report coherent resonant x-ray speckle correlation analysis, which directly determines the reproducibility of CDW domain patterns in  $\text{La}_{1.875}\text{Ba}_{0.125}\text{CuO}_4$  (LBCO 1/8) with thermal cycling. While CDW order is only observed below 54 K, where a structural phase transition results in equivalent Cu-O bonds, we discover remarkably reproducible CDW domain memory upon repeated cycling to temperatures well above that transition. That memory is only lost on cycling across the transition at 240(3) K that restores the four-fold symmetry of the copper-oxide planes. We infer that the structural-domain twinning pattern that develops below 240 K determines the CDW pinning landscape below 54 K. These results open a new view into the complex coupling between charge and lattice degrees of freedom in superconducting cuprates.

Holes doped into the Mott insulating parent compounds of the high temperature superconducting cuprates experience strong interactions with the antiferromagnetic background and with each other, as well as with the lattice in which they reside [1]. The Hubbard Hamiltonian, often used to model the cuprates, predicts that CDW fluctuations are an intrinsic property of strongly interacting electrons in pristine, undistorted 2D square lattices [2, 3]. CDWs have indeed been observed in essentially all hole doped cuprates, but with distinct transition temperatures, correlation lengths and wavevectors [4–11]. This is epitomized by comparing two very similar cuprates that have slightly different low temperature crystal structures:  $\text{La}_{1.875}\text{Sr}_{0.125}\text{CuO}_4$  (LSCO 1/8) and LBCO 1/8. LSCO 1/8 has weak CDW correlations and is a bulk superconductor below its transition temperature of  $T_c = 28$  K [8, 12–15]; whereas LBCO 1/8 has well correlated CDW order that almost completely suppresses bulk superconductivity into what is proposed to be a two dimensional (2D) superconducting pair density wave state [16–20]. As the main difference between these compounds is a subtle change in the crystal structure [21], it is evident the lattice that hosts the CDW correlations has a dramatic influence on the properties of the CDW and the superconducting ground state.

Multiple types of lattice deformation or disorder are present in cuprates including that of interstitial oxygen atoms, chemical substitutions as well as local and long-range tilting of the Cu-O octahedra, all of which have been proposed as possible CDW pinning features that stabilize CDW order [4, 22–28]. One widely discussed lattice deformation in this context is the low temperature tetragonal (LTT) phase in LBCO, in which octahedral tilts define a preferential direction for stripe pinning within each  $\text{CuO}_2$  plane [4, 21, 23]. While the low temperature orthorhombic (LTO) phase is common for both LBCO and LSCO, the LTT structural transition is a special feature in LBCO that coincides with the CDW formation. Fully understanding this process is, however, hampered by a lack of experimental techniques that are sensitive to the phase of the CDW order parameter. To this end, we implemented coherent resonant x-ray speckle correlation analysis as a tool for probing CDW domain pinning in the cuprates, choosing LBCO 1/8 as the model system due to its LTT structure and particularly large CDW correlation length. We discover strikingly reproducible CDW domain formation upon repeated thermal cycling well above its transition temperature and show that the CDW pinning memory is defined by structures that form at the LTO transition rather than disorder or the LTT transition that appears alongside CDW order.

## EXPERIMENT AND RESULTS

Although CDW pinning can dramatically change the superconducting ground state, directly observing CDW pinning and tracking its changes with temperature are very challenging tasks. Much of the difficulty is that one

\* [xmchen@lbl.gov](mailto:xmchen@lbl.gov); Present address: Advanced Light Source, Lawrence Berkeley National Laboratory, Berkeley, CA 94720, USA

† Present address: Stanford Synchrotron Radiation Lightsource, SLAC National Accelerator Laboratory, CA 94025, USA

‡ [mdean@bnl.gov](mailto:mdean@bnl.gov)

§ [swilkins@bnl.gov](mailto:swilkins@bnl.gov)

¶ [irobinson@bnl.gov](mailto:irobinson@bnl.gov)

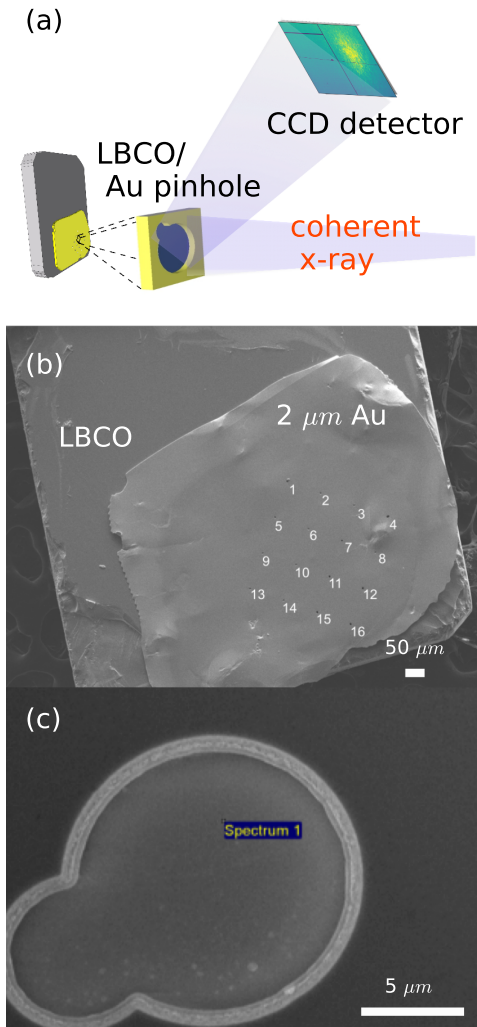


FIG. 1. Experimental setup. (a) The scattering geometry in which coherent x-rays illuminate the masked LBCO 1/8 sample and the CDW Bragg peak is measured on a CCD detector. (b) A SEM image of the LBCO 1/8 single crystal with a Au mask fixed on top. Numbers 1-16 indicate the sixteen pinholes drilled in the Au mask using a focused ion beam (FIB) prior to being fixed on the crystal. (c) A zoomed SEM image of pinhole #10, through which most of our data were taken.

must combine a technique that is sensitive enough to detect the CDW domain spatial arrangement, which we will call “texture”, with the ability to reproducibly illuminate the same sample volume over a wide temperature range. Figure 1 shows how we have addressed the problem using coherent resonant x-ray diffraction: a scattering method that measures the interference between scattering from different domains in the CDW texture as a “speckle” pattern. Our innovation, reported here, is to attach a mask with a microscopic pinhole to the sample, which we overfill with the coherent x-ray beam to ensure we illuminate the same sample volume despite possible temperature induced drifts of the sample position.

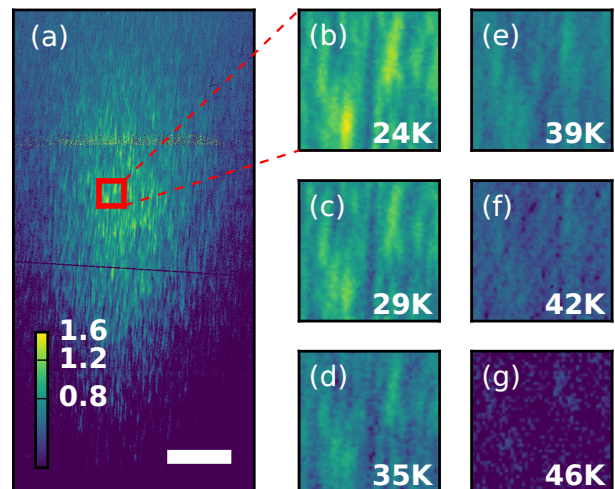


FIG. 2. Temperature dependence of the CDW speckle positions within the ordered state. (a) A detector image of the LBCO 1/8 CDW Bragg peak at 24 K at  $\mathbf{Q} = (0.236, 0, 1.5)$ . The color-bar denotes intensity in photons/second, and the white bar at the bottom indicates 100 detector pixels (0.0025 r.l.u.). (b-g) The temperature dependence of speckle positions as the temperature was raised from 24 to 46 K. Zoomed-in speckle images are taken from the same detector area indicated by the red box in (a). Despite the broadening and weakening of the CDW Bragg peak, the speckles tend to persist in similar locations to 46 K, above which the speckle intensity becomes too low and noise dominates the signal.

An LBCO 1/8 single crystal was aligned to the CDW Bragg condition at wavevector  $\mathbf{Q} = (0.236, 0, 1.5)$  (see Methods). We furthermore tuned the x-ray energy to the Cu  $L_3$ -edge resonance around 931 eV in order to enhance our sensitivity to the weak CDW. In this condition the incident x-ray angle is  $\theta_i = 88^\circ$  with respect to the [001] sample surface and the detector angle is  $2\theta = 119^\circ$ . Such an approach has been used extensively to study the average CDW properties [5–9, 29–31]. The very high coherent flux ( $10^{13}$  photons/s) at the 23-ID-1 beam line at the National Synchrotron Light Source II opens up the possibility of observing coherent interference between the domains of a weakly scattering order parameter such as cuprate CDWs [32, 33]. This was configured to produce a beam of approximately  $20 \mu\text{m}$  at the sample overfilling the  $10 \mu\text{m}$  pinhole in the Au mask attached to the sample (see Methods).

Figure 2(a) plots a detector image at the CDW Bragg condition, which is zoomed in panels (b)-(g). The extent of the observed peak (in this case  $\sim 4 \times 10^{-3} \text{ \AA}^{-1}$ ) is inversely proportional to the CDW correlation length (or domain size) similar to what is seen in conventional scattering. The speckle modulations on top of the peak envelope arise from coherent interference between different CDW domains. The average size and elongated shape of the speckles on the detector is determined primarily

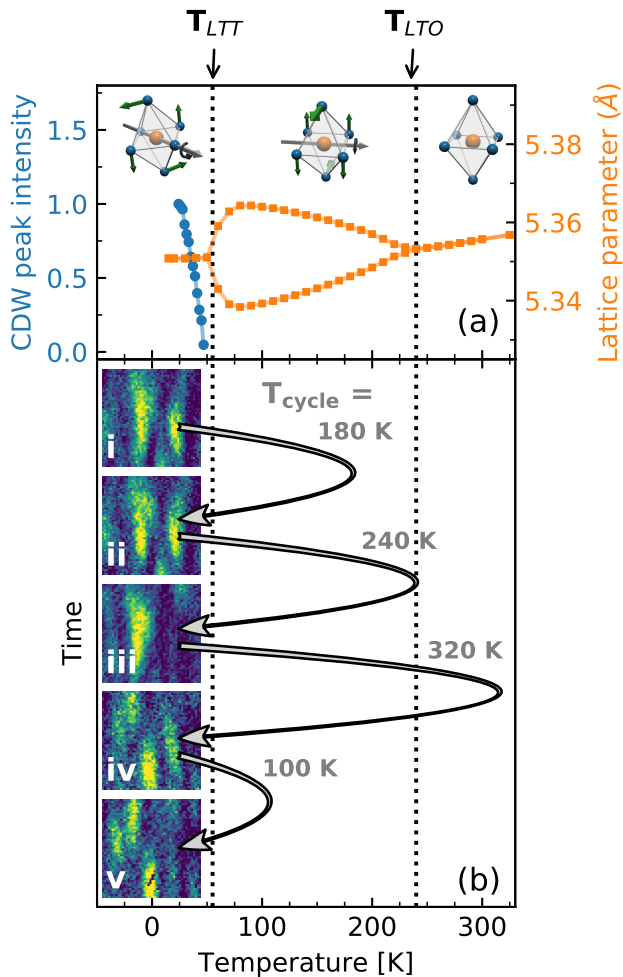


FIG. 3. (a) Temperature dependence of normalized CDW peak intensity (blue) and lattice parameters reproduced from [34] (orange). The CDW transition coincides with the LTT structural transition at  $T_{LTT}$ . A second lattice transition occurs at  $T_{LTO}$ . The inset images represent the octahedral tilts associated with the LTT, LTO and HTT phases. (b) CDW speckle images taken at 24 K. The black arrows indicate the temperature cycling between images.  $T_{\text{cycle}}$  indicates the highest temperature that sample was brought to during a temperature cycle.

by the geometry of the experiment and the extent of the illuminated sample volume, which is fixed by the  $10 \mu\text{m}$  pinhole and  $\sim 100 \text{ nm}$  x-ray penetration depth [Fig. 1(a)] [35]. Therefore, the speckle size and shape do not immediately provide information on the sample properties. The speckle locations, however, are highly sensitive to the CDW domain positions and can therefore be used to test for changes in the CDW domain texture as a function of temperature [36–38]. In LBCO 1/8, static CDW order exists at low temperatures with a correlation length of  $240 \text{ \AA}$ . This can be directly verified with x-rays by noting that the speckle pattern does not vary as a function of time as reported previously [32, 33]. With increas-

ing temperature the CDW correlation length decreases and the CDW Bragg peak disappears coincident with  $T_{LTT} = 54 \text{ K}$  (Fig. S3, [29, 30, 32, 39–41]). The temperature dependence of the CDW peak intensity is explicitly compared with the LTT to LTO structural phase transition in Fig. 3 (a). We measured a range of temperatures from 24 up to 46 K (the highest temperature for which we have sufficient CDW signal in order to observe the speckle locations). At all temperatures, the speckle locations were found to persist as illustrated in Fig. 2(b)-(g).

Next we studied the reproducibility of the CDW domain texture after thermal cycling. Speckle images were taken at 24 K successively before and after the sample temperature was cycled to  $T_{\text{cycle}}$  as we illustrate in Fig. 3 (b). After cycling to  $T_{\text{cycle}} = 180 \text{ K}$ , a temperature well above the CDW transition temperature, the speckle patterns are strikingly similar [see panels (i) and (ii)]. However, as the sample was heated to higher temperatures, the degree of reproducibility dropped, and by  $T_{\text{cycle}} = 320 \text{ K}$ , their positions completely changed as seen in panels (ii) to (iv).

In order to quantitatively compare speckle positions, and identify the onset temperature of this change, we calculated the normalized cross-correlation function. Speckle images were background subtracted as described in the Supplementary Information Section S1. These images are then represented as  $M \times N$  matrices  $A_{m,n}$  and  $B_{m,n}$  where  $m$  and  $n$  are row-column indices. Cross-correlations matrices are calculated via

$$A_{m,n} * B_{m,n} = \sum_{m'=-M}^M \sum_{n'=-N}^N A_{m',n'} B_{m+m',n+n'}. \quad (1)$$

Here,  $A_{m,n}$  and  $B_{m,n}$  were taken to be  $M = 200 \times N = 200$ -pixel images under the CDW peak measured before and after thermally cycling the sample, which include  $\sim 30 - 50$  speckles. When  $A_{m,n}$  and  $B_{m,n}$  have the same or similar speckle patterns, the correlated intensity features a peak that we sum over to obtain a single normalized speckle cross-correlation coefficient [36–38]

$$\xi = \frac{\sum_{\text{speckle}} A_{m,n} * B_{m,n}}{\left( \sum_{\text{speckle}} A_{m,n} * A_{m,n} \sum_{\text{speckle}} B_{m,n} * B_{m,n} \right)^{1/2}}. \quad (2)$$

In this equation,  $\sum_{\text{speckle}}$  denotes summing over the peak in the cross-correlation matrix, corresponding to just over one speckle ( $\sim 4 \times 16$  pixels) in size. The value is normalized by dividing by the auto-correlations of  $A_{m,n}$  and  $B_{m,n}$ , such that two identical images have  $\xi = 1$ . In Fig. 4, we show  $\xi$  for various cycle temperatures showing a transition from high to low speckle reproducibility well above the CDW ordering temperature. We fit  $\xi$  versus  $T_{\text{cycle}}$  using an error function, which provides a reasonable phenomenological description of the shape of the transition. The onset temperature of de-correlation

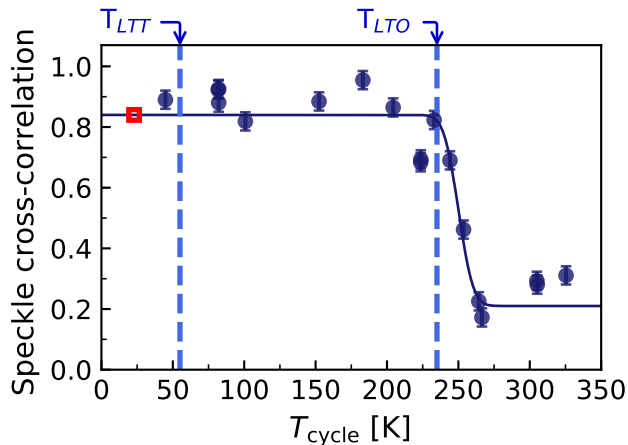


FIG. 4. Normalized speckle cross-correlation coefficient,  $\xi$ , of data before and after temperature cycling to different values of  $T_{\text{cycle}}$ . Images of  $200 \times 200$  detector pixels were used for this calculation. An error function fit gives a de-correlation onset temperature of 240(3) K, which coincides with the LTO structural phase transition. The red box indicates 24 K the temperature where all the speckle images were sampled for this figure. Error bars are estimated by taking the standard deviation of repeated, nominally equivalent, measurements.

was 240(3) K, which coincides with the LTO structural phase transition at  $T_{\text{LTO}} = 236(5)$  K [39]. This transition involves rotations of the Cu-O octahedra around the  $\langle 110 \rangle_{\text{HTT}}$  direction and since nearest-neighbor octahedra rotate in opposite directions, the unit cell volume increases by a factor of two, with  $a_o \approx b_o \approx \sqrt{2}a$ . Below this threshold the majority of the speckles reproduce with  $\xi = 0.84(9)$ ; above the transition  $\xi = 0.21(4)$ , which corresponds to the value expected in a random domain distribution as estimated by computing  $\xi$  after flipping one of the images about a horizontal axis. We further confirmed that different regions within the speckle pattern shown in Fig. 2(a) and data taken through another pinhole reproduce the same phenomenology within error bars.

## DISCUSSION

This work establishes that the CDW domains are strikingly reproducible upon temperature cycling well above the LTT and CDW transitions, up to  $T_{\text{cycle}} = 240(3)$  K. Disorder and structural distortions are present in almost all cuprates and have been discussed extensively in connection with CDW pinning in the cuprates [4, 22–28, 42]. In  $\text{La}_{2-x}\text{Ba}_x\text{CuO}_4$  the most prominent form of disorder is La/Ba cation substitution and the most obvious structural features come from the LTO and LTT phase domain boundaries.

Random La/Ba distribution, or other forms of chemical disorder, appear to play a role in pinning the CDW

into a static ground state and in setting an upper limit on the CDW correlation length [25–27, 32, 42]. Chemical disorder such as this will, however, always be fixed at all temperature considered in this study and therefore cannot explain the sharp transition in the observed memory effect upon cycling above 240 K.

In the context of structural CDW pinning, the importance of the LTT phase has been emphasized since the discovery of CDW order in the cuprates [4]. This phase features rows of oxygen atoms along the  $\langle 100 \rangle_{\text{HTT}}$  directions displaced in/out of the  $\text{CuO}_2$  planes, which appear particularly suitable for pinning [4, 21, 43]. The concomitance of the CDW and LTT transitions, as well as the particularly long CDW correlation length in LBCO and  $\text{La}_{1.6-x}\text{Nd}_{0.4}\text{Sr}_x\text{CuO}_4$  relative to other cuprates such as LSCO, is surely due to coupling between the LTT and CDW phases [4, 8, 10, 30, 40, 41, 44, 45]. It is, consequently, highly intriguing that the CDW memory persists well above this transition. Figure 4 shows a sharp cross-over from near-complete to minimal reproducibility at 240(3) K. This threshold temperature coincides with the LTO phase transition at 236(5) K [34, 39], implying that the pinning configuration is effectively determined at this phase transition, where octahedral tilts break the four-fold symmetry of copper-oxide planes. At this LTO transition LTO twin domain boundaries form. Based on strain considerations, these are expected to occur along the  $\langle 100 \rangle_{\text{HTT}}$  lattice directions, as confirmed by transmission electron microscopy (TEM) imaging [46–48]. Early structural studies of LBCO demonstrated that the LTT and LTO tilt patterns can be conceptualized as superpositions of one-another [21, 43] and superposition-based arguments naturally justified the observation that LTT-like tilts occur at LTO domain boundaries in the cuprates [46–48]. This interaction opens the possibility that the LTT domain boundary configuration can be inherited from the LTO domain boundary configuration. This would explain how the CDW onset temperature coincides with the LTT transition, but the memory effect matches the LTO transition.

Another significant observation is that, within the CDW phase, the speckle locations do not change with temperature (see Fig. 2), despite the fact that the CDW correlation length varies with temperature [10, 30, 39, 40, 44]. This can be explained by uniform expansion of CDW domains around their pinning centers on cooling, as speckle locations are primarily dependent on the locations of the domains and largely insensitive to their size (see Supplementary Information Section S3).

Almost all cuprates show some form of orthorhombic structural symmetry breaking, so the CDW memory effects discovered here may well be shared by many different cuprate species. Testing whether other cuprates, including those without a LTT phase, show similar behavior will be important in future work. We further emphasize that the experimental configuration presented here, in which sample drift problems are avoided by attaching a mask directly to the sample, is also applicable to ap-



plied current or laser excitation as well as to the magnetic field dependent behavior studied previously in magnetic alloys [36–38]. This complements what can be achieved with scanning tunneling spectroscopy, which has superior spatial resolution, but is limited to cleaved surfaces [24]. The use of coherence and resonant x-ray scattering further opens the possibility to study charge, spin and orbital order parameters in other quantum materials with better resolution than is possible with current microdiffraction techniques [27].

In conclusion, we present the first application of coherent resonant soft x-ray speckle correlation analysis to study the CDW domain hysteresis in LBCO 1/8. We uncover remarkably reproducible CDW domain formation upon temperature cycling far above the 54 K CDW transition, before the CDW pattern is almost completely reconfigured by cycling above 240(3) K. The CDW order, which is associated with the dramatic suppression of superconductivity in this sample, experiences a pinning landscape that is determined by structural domains that form at the LTO phase transition. Our results open a new route to studying the complex interplay between lattice and charge degrees of freedom in quantum materials at cryogenic temperatures.

## METHODS

### Sample preparation

Single crystals of LBCO 1/8 were grown using the floating zone method, and characterized extensively in previous studies [10, 11, 30, 41, 49], all indicating excellent sample quality. A 2  $\mu\text{m}$  gold (Au) film was evaporated onto a free-standing 200 nm  $\text{Si}_3\text{N}_4$  membrane. Ar-

rays of 10  $\mu\text{m}$  asymmetric pinholes were drilled into the film using a focused ion beam yielding the shape shown in Fig. 1 (c) [50]. This assembly was pressed onto the LBCO single crystal with Poly Methyl Methacrylate (PMMA) as a glue. The excess PMMA that filled in the pinholes was then removed using reactive ion etching. The resulting sample was imaged in a JEOL 7600F scanning electron microscope [Fig. 1, (b) and (c)]. In this paper we index the crystal using the HTT unit cell where  $a = b = 3.78$  and  $c = 13.28$  Å. Correlation length here is defined as  $a/\text{HWHM}$  where HWHM is the half width at half maximum of the peak in r.l.u.

### X-ray scattering and Imaging

Data were taken at the 23-ID-1 beamline at the National Synchrotron Light Source II (NSLS II) which is optimized to deliver high coherent flux at the sample. The beam was energy-dispersed in the vertical plane with a grating and focused onto a 20  $\mu\text{m}$  pinhole approximately 5 mm from the sample to which the Au mask with a 10  $\mu\text{m}$  pinhole was attached. In this configuration, the transverse coherence of the beam is greater than the extent of the illuminated region of the sample and the longitudinal coherence of the beam is of order 2  $\mu\text{m}$ . The X-ray energy was further tuned to the Cu  $L_3$  absorption edge around 931 eV to enhance the signal from the CDW peak. The positions of the pinholes were determined by scanning the sample through the X-ray beam using the LBCO Cu fluorescent yield. Data were collected using a fast CCD [51] with a  $30 \times 30 \mu\text{m}^2$  pixel size placed 340 mm from the sample. Images were read out every 5 s for a total collection time of approximately 10 min.

- 
- [1] Keimer, B., Kivelson, S., Norman, M., Uchida, S. & Zaanen, J. From quantum matter to high-temperature superconductivity in copper oxides. *Nature* **518**, 179–186 (2015).
  - [2] Zheng, B.-X. *et al.* Stripe order in the underdoped region of the two-dimensional hubbard model. *Science* **358**, 1155–1160 (2017).
  - [3] Huang, E. W. *et al.* Numerical evidence of fluctuating stripes in the normal state of high- $c$  cuprate superconductors. *Science* **358**, 1161–1164 (2017).
  - [4] Tranquada, J. M., Sternlieb, B. J., Axe, J. D., Nakamura, Y. & Uchida, S. Evidence for stripe correlations of spins and holes in copper oxide superconductors. *Nature* **375**, 561–563 (1995).
  - [5] Ghiringhelli, G. *et al.* Long-range incommensurate charge fluctuations in  $(\text{Y,Nd})\text{Ba}_2\text{Cu}_3\text{O}_{6+x}$ . *Science* **337**, 821–825 (2012).
  - [6] Comin, R. *et al.* Charge order driven by fermi-arc instability in  $\text{Bi}_2\text{Sr}_{2-x}\text{La}_x\text{CuO}_{6+\delta}$ . *Science* **343**, 390–392 (2014).
  - [7] da Silva Neto, E. H. *et al.* Ubiquitous interplay between charge ordering and high-temperature superconductivity in cuprates. *Science* **343**, 393–396 (2014).
  - [8] Thampy, V. *et al.* Rotated stripe order and its competition with superconductivity in  $\text{La}_{1.88}\text{Sr}_{0.12}\text{CuO}_4$ . *Phys. Rev. B* **90**, 100510 (2014).
  - [9] Tabis, W. *et al.* Charge order and its connection with fermi-liquid charge transport in a pristine high- $T_c$  cuprate. *Nature Communications* **5** (2014).
  - [10] Miao, H. *et al.* High-temperature charge density wave correlations in  $\text{La}_{1.875}\text{Ba}_{0.125}\text{CuO}_4$  without spin-charge locking. *Proceedings of the National Academy of Sciences* **114**, 12430–12435 (2017).
  - [11] Miao, H. *et al.* Incommensurate phonon anomaly and the nature of charge density waves in cuprates. *Phys. Rev. X* **8**, 011008 (2018).
  - [12] Croft, T. P., Lester, C., Senn, M. S., Bombardi, A. & Hayden, S. M. Charge density wave fluctuations in  $\text{La}_{2-x}\text{Sr}_x\text{CuO}_4$  and their competition with superconductivity. *Phys. Rev. B* **89**, 224513 (2014).

- [13] Christensen, N. *et al.* Bulk charge stripe order competing with superconductivity in  $\text{La}_{2-x}\text{Sr}_x\text{CuO}_4$  ( $x = 0.12$ ). *arXiv preprint arXiv:1404.3192* (2014).
- [14] Wu, H.-H. *et al.* Charge stripe order near the surface of 12-percent doped  $\text{La}_{2-x}\text{Sr}_x\text{CuO}_4$ . *Nature Communications* **3**, 1023 (2012).
- [15] It is possible that the weak CDW order in LSCO 1/8 is only present due to local LTT like tilts or the presence of a low temperature less orthorhombic structural phase [52, 53].
- [16] Moodenbaugh, A. R., Xu, Y., Suenaga, M., Folkerts, T. J. & Shelton, R. N. Superconducting properties of  $\text{La}_{2-x}\text{Ba}_x\text{CuO}_4$ . *Phys. Rev. B* **38**, 4596–4600 (1988).
- [17] Li, Q., Hücker, M., Gu, G. D., Tsvelik, A. M. & Tranquada, J. M. Two-dimensional superconducting fluctuations in stripe-ordered  $\text{La}_{1.875}\text{Ba}_{0.125}\text{CuO}_4$ . *Phys. Rev. Lett.* **99**, 067001 (2007).
- [18] Berg, E. *et al.* Dynamical layer decoupling in a stripe-ordered high- $T_c$  superconductor. *Phys. Rev. Lett.* **99**, 127003 (2007).
- [19] Fradkin, E., Kivelson, S. A. & Tranquada, J. M. *Colloquium* : Theory of intertwined orders in high temperature superconductors. *Rev. Mod. Phys.* **87**, 457–482 (2015).
- [20] Xu, Z. *et al.* Neutron-scattering evidence for a periodically modulated superconducting phase in the underdoped cuprate  $\text{La}_{1.905}\text{Ba}_{0.095}\text{CuO}_4$ . *Phys. Rev. Lett.* **113**, 177002 (2014).
- [21] Axe, J. D. *et al.* Structural phase transformations and superconductivity in  $\text{La}_{2-x}\text{Ba}_x\text{CuO}_4$ . *Phys. Rev. Lett.* **62**, 2751–2754 (1989).
- [22] Božin, E., Billinge, S., Kwei, G. & Takagi, H. Charge-stripe ordering from local octahedral tilts: Underdoped and superconducting  $\text{La}_{2-x}\text{Sr}_x\text{CuO}_4$  ( $0 \leq x \leq 0.30$ ). *Physical Review B* **59**, 4445 (1999).
- [23] Kivelson, S. A. *et al.* How to detect fluctuating stripes in the high-temperature superconductors. *Rev. Mod. Phys.* **75**, 1201–1241 (2003).
- [24] Hanaguri, T. *et al.* A checkerboard?electronic crystal state in lightly hole-doped  $\text{Ca}_{2-x}\text{Na}_x\text{CuO}_2\text{Cl}_2$ . *Nature* **430**, 1001–1005 (2004).
- [25] Vojta, M. Lattice symmetry breaking in cuprate superconductors: stripes, nematics, and superconductivity. *Advances in Physics* **58**, 699–820 (2009).
- [26] Nie, L., Tarjus, G. & Kivelson, S. A. Quenched disorder and vestigial nematicity in the pseudogap regime of the cuprates. *Proceedings of the National Academy of Sciences* **111**, 7980–7985 (2014).
- [27] Campi, G. *et al.* Inhomogeneity of charge-density-wave order and quenched disorder in a high- $T_c$  superconductor. *Nature* **525**, 359–362 (2015).
- [28] Wu, T. *et al.* Incipient charge order observed by NMR in the normal state of  $\text{YBa}_2\text{Cu}_3\text{O}_y$ . *Nature communications* **6** (2015).
- [29] Abbamonte, P. *et al.* Spatially modulated ‘Mottness’ in  $\text{La}_{2-x}\text{Ba}_x\text{CuO}_4$ . *Nature Physics* **1**, 155–158 (2005).
- [30] Wilkins, S. B. *et al.* Comparison of stripe modulations in  $\text{La}_{1.875}\text{Ba}_{0.125}\text{CuO}_4$  and  $\text{La}_{1.48}\text{Nd}_{0.4}\text{Sr}_{0.12}\text{CuO}_4$ . *Phys. Rev. B* **84**, 195101 (2011).
- [31] Hashimoto, M. *et al.* Direct observation of bulk charge modulations in optimally doped  $\text{Bi}_{1.5}\text{Pb}_{0.6}\text{Sr}_{1.54}\text{CaCu}_2\text{O}_{8+\delta}$ . *Phys. Rev. B* **89**, 220511 (2014).
- [32] Chen, X. M. *et al.* Remarkable stability of charge density wave order in  $\text{La}_{1.875}\text{Ba}_{0.125}\text{CuO}_4$ . *Phys. Rev. Lett.* **117**, 167001 (2016).
- [33] Thampy, V. *et al.* Static charge-density-wave order in the superconducting state of  $\text{La}_{2-x}\text{Ba}_x\text{CuO}_4$ . *Phys. Rev. B* **95**, 241111 (2017).
- [34] Bozin, E. S. *et al.* Reconciliation of local and long-range tilt correlations in underdoped  $\text{La}_{2-x}\text{Ba}_x\text{CuO}_4$  ( $0 \leq x \leq 0.155$ ). *Phys. Rev. B* **91**, 1–13 (2015). 1412.6513.
- [35] See Ref. [32, 33] for a detailed discussion of the speckle shape and speckle visibility.
- [36] Pierce, M. S. *et al.* Quasistatic X-Ray Speckle Metrology of Microscopic Magnetic Return-Point Memory. *Phys. Rev. Lett.* **90**, 175502–175504 (2003).
- [37] Chesnel, K., Nelson, J., Wilcken, B. & Kevan, S. D. Mapping spatial and field dependence of magnetic domain memory by soft X-ray speckle metrology. *Journal of Synchrotron Radiation* **19**, 293–306 (2012).
- [38] Chesnel, K., Safsten, A., Rytting, M. & Fullerton, E. E. Shaping nanoscale magnetic domain memory in exchange-coupled ferromagnets by field cooling. *Nature Communications* **7**, 11648 (2016).
- [39] Hücker, M. *et al.* Stripe order in superconducting  $\text{La}_{2-x}\text{Ba}_x\text{CuO}_4$  ( $0.095 \leq x \leq 0.155$ ). *Phys. Rev. B* **83**, 104506 (2011).
- [40] Hücker, M. *et al.* Enhanced charge stripe order of superconducting  $\text{La}_{2-x}\text{Ba}_x\text{CuO}_4$  in a magnetic field. *Phys. Rev. B* **87**, 014501 (2013).
- [41] Dean, M. P. M. *et al.* Magnetic excitations in stripe-ordered  $\text{La}_{1.875}\text{Ba}_{0.125}\text{CuO}_4$  studied using resonant inelastic x-ray scattering. *Phys. Rev. B* **88**, 020403 (2013).
- [42] Alloul, H., Bobroff, J., Gabay, M. & Hirschfeld, P. J. Defects in correlated metals and superconductors. *Rev. Mod. Phys.* **81**, 45–108 (2009).
- [43] Hücker, M. Structural aspects of materials with static stripe order. *Physica C: Superconductivity* **481**, 3–14 (2012).
- [44] Fujita, M., Goka, H., Yamada, K., Tranquada, J. M. & Regnault, L. P. Stripe order, depinning, and fluctuations in  $\text{La}_{1.875}\text{Ba}_{0.125}\text{CuO}_4$  and  $\text{La}_{1.875}\text{Ba}_{0.075}\text{Sr}_{0.050}\text{CuO}_4$ . *Phys. Rev. B* **70**, 104517 (2004).
- [45] Baity, P. G., Sasagawa, T. & Popović, D. Collective dynamics and strong pinning near the onset of charge order in  $\text{La}_{1.48}\text{Nd}_{0.4}\text{Sr}_{0.12}\text{CuO}_4$ . *Phys. Rev. Lett.* **120**, 156602 (2018).
- [46] Zhu, Y. *et al.* Tetragonal-orthorhombic structural modulation at low temperature in  $\text{La}_{2-x}\text{Ba}_x\text{CuO}_4$ . *Phys. Rev. Lett.* **73**, 3026–3029 (1994).
- [47] Chen, C., Cheong, S., Werder, D., Cooper, A. & Rupp, L. Low temperature microstructure and phase transitions in  $\text{La}_{2-x}\text{Sr}_x\text{CuO}_4$  and  $\text{La}_{2-x}\text{Ba}_x\text{CuO}_4$ . *Physica C: Superconductivity* **175**, 301–309 (1991).
- [48] Chen, C., Cheong, S.-W., Werder, D. & Takagi, H. Microstructural changes induced by lattice instabilities in  $\text{La}_{2-x}\text{Ba}_x\text{CuO}_4$  ( $x = 0.125$ ) and  $\text{Nd}_2\text{NiO}_4$ . *Physica C: Superconductivity* **206**, 183–194 (1993).
- [49] Thampy, V. *et al.* Comparison of charge modulations in  $\text{La}_{1.875}\text{Ba}_{0.125}\text{CuO}_4$  and  $\text{YBa}_2\text{Cu}_3\text{O}_{6.6}$ . *Phys. Rev. B* **88**, 024505 (2013).
- [50] Although any stable shape is adequate for speckle correlation analysis, we chose to make a two-lobe structure. This decision was taken to break circular symmetry, which should improve the prospects for obtaining real-space images via Bragg Coherent Diffractive Imaging in

the future. Such attempts have thus far been unsuccessful.

- [51] Doering, D. *et al.* Development of a compact fast ccd camera and resonant soft x-ray scattering endstation for time-resolved pump-probe experiments. *Review of Scientific Instruments* **82** (2011).
- [52] Božin, E., Kwei, G., Takagi, H. & Billinge, S. Neutron diffraction evidence of microscopic charge inhomogeneities in the  $\text{CuO}_2$  plane of superconducting  $\text{La}_{2-x}\text{Sr}_x\text{CuO}_4$  ( $0 \leq x \leq 0.30$ ). *Phys. Rev. Lett.* **84**, 5856 (2000).
- [53] Jacobsen, H. *et al.* Neutron scattering study of spin ordering and stripe pinning in superconducting  $\text{La}_{1.93}\text{Sr}_{0.07}\text{CuO}_4$ . *Phys. Rev. B* **92**, 174525 (2015).

### ACKNOWLEDGMENTS

We thank Derek Meyers for useful comments. The work at Brookhaven National Laboratory was supported by the U.S. Department of Energy, Office of Basic Energy Sciences, Division of Materials Sciences and Engineering, under Contract No. DE-SC0012704. This research used resources 23-ID-1 beamline of the National Synchrotron Light Source II, a U.S. Department of Energy (DOE) Office of Science User Facility operated for the DOE Office of Science by Brookhaven National Lab-

oratory under Contract No. DE-SC0012704. The sample pattern was performed at the Center for Functional Nanomaterials, which is a U.S. DOE Office of Science Facility, at Brookhaven National Laboratory under Contract No. DE-SC0012704. Work at Argonne National Laboratory was supported by the US Department of Energy, Office of Basic Energy Sciences, under Contract no. DE-AC0206CH11357.

### Author contributions

S.B.W., M.P.M.D., and I.K.R. initiated and managed the project. X.M.C., C.M., Y.C., V.T., A.M.B., W.H., T.A., H.M., G.F., M.P.M.D., S.B.W., and I.K.R. prepared and performed the x-ray experiment. X.M.C, M.L. and G.D.G. prepared the sample. X.M.C., C.M., Y.C., V.T., J.M.T., M.P.M.D., S.B.W., and I.K.R. analyzed and interpreted the results. X.M.C., M.P.M.D., and I.K.R. wrote the manuscript.

### Competing financial interests

The authors declare no competing financial interests.